# REPORT 2: INVESTIGATION OF ACTIVE FLOW CONTROL AROUND A NACA84-M AEROFOIL

*Liam Huckle*

## 1. INTRODUCTION

The purpose of this CFD analysis is to determine the advantage of active flow control wing designs. The report will compare the performance properties of a wing with and without active flow devices at various angles of attack.

## 2. GEOMETRY AND BOUNDARY CONDITIONS

### 2.1 Geometry

**Figure 1:** Aerofoil NACA84-M showing jet location.

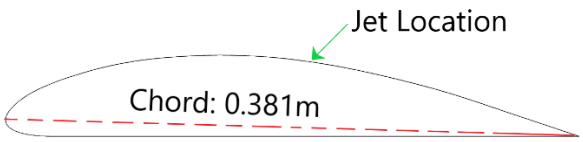


In figure 1, the NACA84-M aerofoil is shown with a chord length of 0.381m. On the suction surface (top surface), a high-velocity jet is placed at 53.9% of the length of the chord from the leading edge. The slot is 0.667% the length of the chord.

**Figure 2:** Solution domain

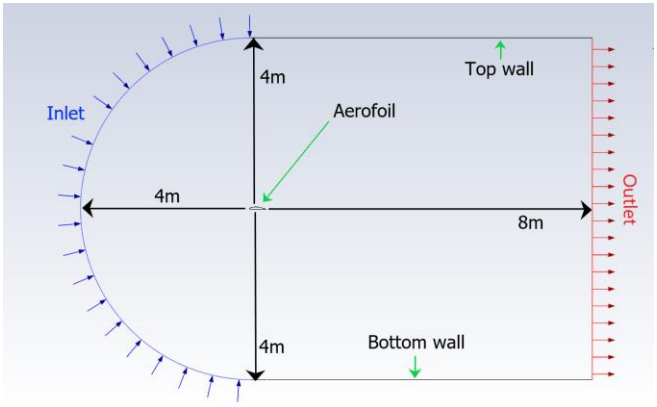


In figure 2, the solution domain is displayed. The fluid domain was heavily influenced by the mesh design that best captures the geometry. This C-type meshing is why the inlet is a radius of 4m from the leading edge. The top and bottom of the domain are wall boundaries. Finally, an outlet is 8m downstream of the trailing edge. The wall boundaries, inlet and outlet were all placed far away from the aerofoil to minimise wall effects and/or possible interference with the flow around the wing. The outlet was made long enough to ensure that the fluid flow was fully developed before exiting the outlet.

### 2.2 Boundary Conditions (inlet, outlet, wall)

#### 2.2.1 Walls

Stationary and a no-slip and condition was set for all boundary walls and the aerofoil to account for zero fluid velocity of the fluid in immediate contact with the surfaces. This is an assumption as particularly with high turbulence rates, synonymous with high angles of attack (AoA) the immediate boundary layer may have velocity and 'slip'.

#### 2.2.2 Inlet

The inlet velocity was calculated as a function of the Reynolds number (1) provided and the properties of the fluid domain. The 'H' variable for the case of an aerofoil investigation is substituted for the chord length.

$$R_e = \frac{\rho U_\infty H}{\mu} \quad (1)$$

$$445\,000 = \frac{1.2256 * (U_\infty) * 0.381}{(1.7894e-05)}$$

$$U_\infty = 17.05272\ m/s$$

The method in which the AoA of the aerofoil was adjusted in Ansys was by altering the velocity vector of the inlet. This meant that the same mesh can be used to evaluate all AoAs of interest. For different angles of attack, the X and Y components of the velocity were calculated using trigonometry and then input into the inlet properties. Cosine and Sine of the input AoA produces the respective X-component and Y-component of the velocity vector.



Liam Huckle mn19lth@leeds.ac.uk 201355349

The orientation of the aerofoil chord was not parallel to the x-axis in Ansys. This is because of the x-axis in the coordinates file which is parallel to the bottom surface and not the chord line. This is simply solved by subtracting the chord angle ($1.627^0$) relative to the x-axis in the coordinates file, from the intended AoA. It is this new corrected AoA that is input to the inlet conditions. (Note: The chord angle used is of the mesh file which deviates from section **2.1** this is explained further in **3.1**).

### 2.2.3 Airjet (Inlet slot)

The inlet velocity of the jet is set to 12 times the free stream. This produces a velocity of 204.63 m/s. To replicate the jet vectoring at a tangent to the aerofoil surface, the angle of declination of the surface was found using trigonometry and the two co-ordinates sets (point 40 & 41). The X and Y components of the velocity were calculated and then entered into the inlet condition of the slot inlet.

### 2.2.4 Outlet

The outlet had a gauge pressure of zero Pa assigned to simulate atmospheric pressure. The turbulence intensity was set to match the inlet.

### 2.2.5 Turbulence Intensity

For simplicity, the flow is considered external due to the distance of the inlet, walls and outlet to the aerofoil. An intensity and length method of turbulence was employed. The given value of I = 0.1 was used and the length $L_T$ = 0.07*(Chord) = 0.02667. This value was applied for both outlet and inlet as well as the air jet. The fluid used was air and the default Fluent properties were used including the density of 1.225 $Kg/m^3$ and viscosity of 1.7894e-05 Kg/ms.

## 3. MESH DESIGN

### 3.1 Structured Mesh

As mentioned, a C-type meshing method was employed to best capture the curvature of the aerofoil while maintain good cell quality. This is a structured quad style mesh. It should be noted that the mesh dimensions deviate from the initial geometry to aid in the grid alignment. The trailing edge was removed, and the resultant 'blunt edge' was extruded at a tangent to the wing until a new trailing edge was formed.

Figure 3 illustrates the trailing edge before and after extrusion. The trailing edge now sits flush with the bottom surface; however, the chord length has increased to 0.3919m in length (leading edge to trailing edge). The angle between the chord line and the bottom flat surface is also different and is accounted for in the inlet condition velocity vectors explained in **2.2.2**.

**Figure 3:** Trailing edge adaption

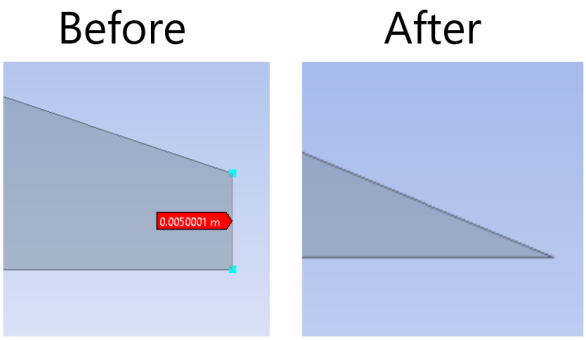


### 3.2 Segmentation of the Fluid Domain

To aid in grid alignment the fluid domain was split into sections. The border lines formed, created a line segment that the Mesher could select and apply the desired number of cell divisions and biases. This is illustrated in figure 4.

**Figure 4:** View of the cell divisions and bias applied, highlighting the 6 split sections.

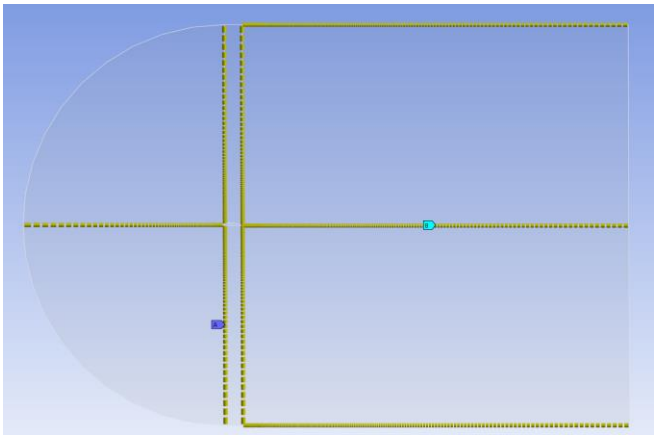



Liam Huckle mn19lth@leeds.ac.uk 201355349

### 3.2 Cell refinement

As a general rule, more cell refinement was placed anywhere that fluid property gradients were expected to be greatest. Naturally for an aerofoil this is the region just before the leading edge, around the surfaces and a distance behind the trailing edge. Since the air-jets velocity is so large a further cell refinement was done in the region around the slot.

**Figure 5:** Increased cell count located by the jet inlet.

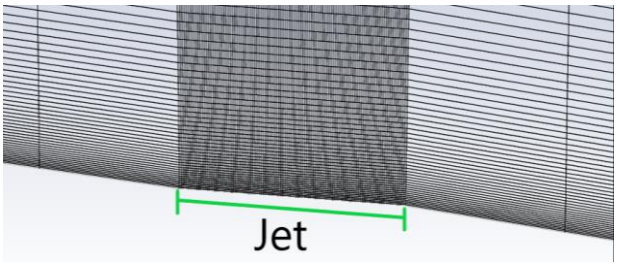


This was accomplished by using 'number of divisions' on the aerofoil sections and borders of face segments. A heavy bias was applied so that majority of the cells were clustered in the regions specified above. The number of divisions was adjusted until sufficient resolution was achieved. The Bias was adjusted until the desired first cell thickness was achieved.

**Figure 6:** Fine mesh

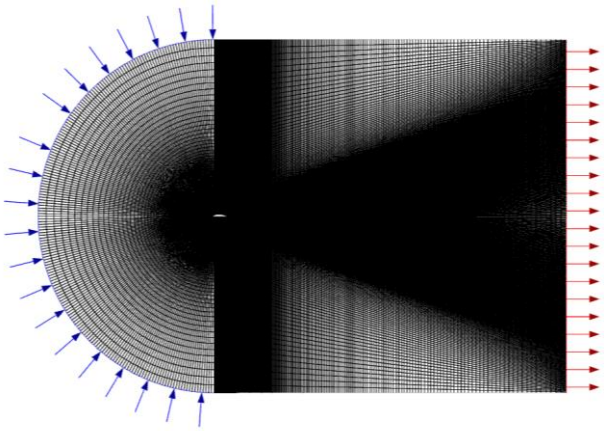

**Figure 7:** Fine mesh zoomed.

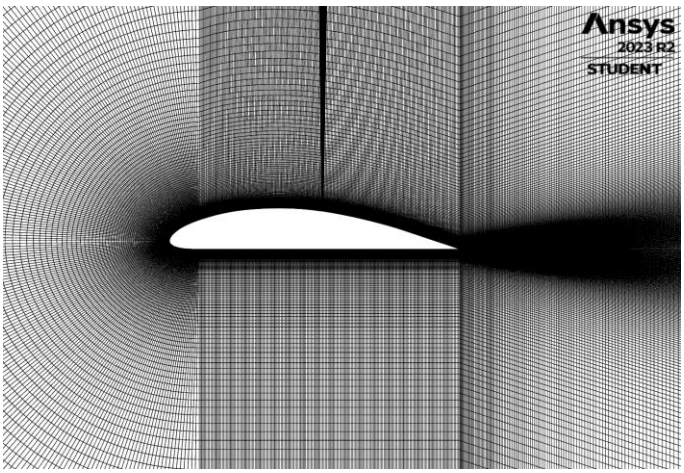


### 3.3 Y+ Value

The bias of the cell divisions was adjusted until a desired wall spacing was reached so that a Y+ value of approximately 1 was achieved. The wall spacing value was calculated using an online Y+ Calculator [1]. Table 1 compares the desired wall spacing with the wall spacing of the mesh models.

**Table 1:** Wall spacing comparison (units are millimetres)

| Mesh | Wall spacing | Desired wall spacing | ΔDelta |
|---|---|---|---|
| Coarse | 0.01900 | 0.01901 | -0.00010 |
| Coarse-Medium | 0.02000 | 0.01901 | 0.00099 |
| Medium | 0.02000 | 0.01901 | 0.00099 |
| Fine | 0.01900 | 0.01901 | -0.00010 |

### 3.4 Mesh Independence

Using the three finest meshes defined above, a mesh independence study was conducted for the $0^0$ AoA scenario on the normal wing with no flow control. The GCI equation (2) will be used to quantify the discretisation error.

$$GCI = \frac{Fs|e|}{r^p - 1} \quad (2)$$

'Fs' is given as safety factor of 3 due to the uncertainty of results. 'e' is the difference in variable solutions and calculated using (3).

$$e = \frac{f_2 - f_1}{f_1} \quad (3)$$



Liam Huckle mn19lth@leeds.ac.uk 201355349

'r' is the grid refinement ratio calculated using (4).

$$r_{eff} = \left(\frac{N_1}{N_2}\right)^{\frac{1}{D}} \quad (4)$$

and 'p' is the formal order of accuracy given to be 2 for second order simulations. (This isn't always the case and is usually less than 2)

**Table 2:** Summary of GCI Index

| Mesh | N, cells | Lift (N) | \|e\| | $r_{eff}$ | GCI (%) |
|---|---|---|---|---|---|
| Coarse-Medium | 65800 | 36.309582 | n/a | n/a | n/a |
| Medium | 147900 | 36.31335 | 0.000104 | 1.4992 | 0.0249 |
| Fine | 263000 | 36.374428 | 0.001679 | 1.3335 | 0.6472 |

**Figure 8:** Graph of grid sensitivity, showing convergence.

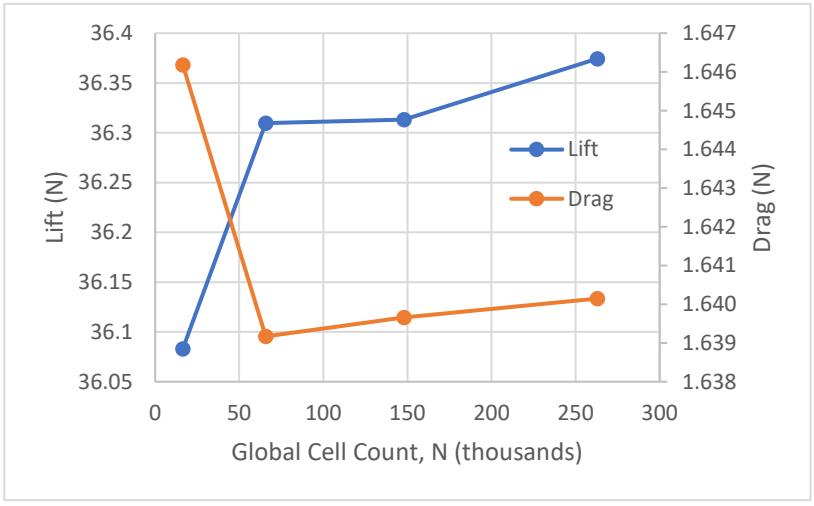


The highest cell count mesh was used for increased accuracy even though it could be argued the medium mesh could be used due to how similar the output values were and the values converging as seen in figure 8.

## 4. SOLVER SETTINGS

### 4.1 Viscous Model

The K-Omega SST model was employed so that turbulent length scales in the boundary layer adjacent to the aerofoil surface could be resolved. The SST K-Omega model uses the k-ε model in the freestream and K-ω in the boundary layer. This is because the different models are optimised for different regions of flow. K-Omega needs a y+ ≈1 which was achieved in the mesh and the enhanced wall treatment was enabled in the solver to help capture the boundary layer.

### 4.2 Solution Methods

A pressure-velocity coupling scheme was utilised since the flow is assumed to be incompressible. Another assumption is that the flow is steady state not transient. For high AoAs this might not be the case and could lead to inaccuracies.

A Green-Gauss Cell Based method was utilised as this method works best for structured hexahedral meshes. The spatial discretization terms were set to second order upwind for an increased level of accuracy.

To initialise the simulations a hybrid initialisation was used for the first AoA investigated and then that result was used to initialise the following simulated AoA. This was repeated until the last AoA was simulated. This was used as a time saving solution as initialisation is not necessary when the previous result can be used as a starting point.

### 4.3 Reference Values

The chord length of 0.381m and density of air, 1.225 kg/m$^3$ was input into the reference values section.

## 5. RESULTS AND ANALYSIS

### 5.1 Parameters of Interest

Following each simulation, the forces in the X and Y direction were tabulated. These were relative to the reference frame and not the AoA, hence a correction calculation was made to calculate lift and drag which are perpendicular (lift) and parallel (drag) to the free stream.



Liam Huckle mn19lth@leeds.ac.uk 201355349

### 5.2 Validation Results

**Figure 9:** Comparison of Coefficient of Lift of CFD and experimental data.

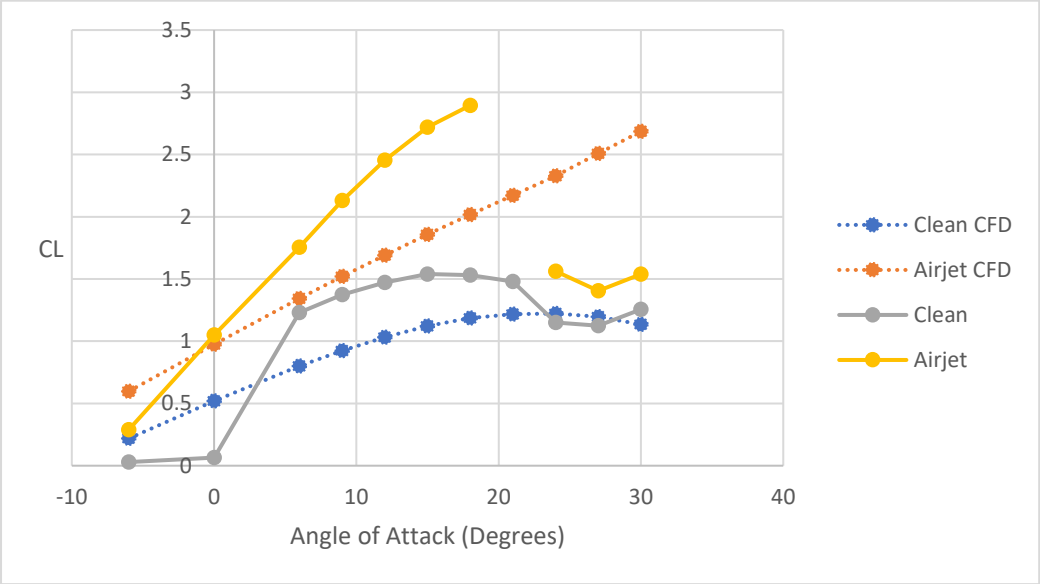


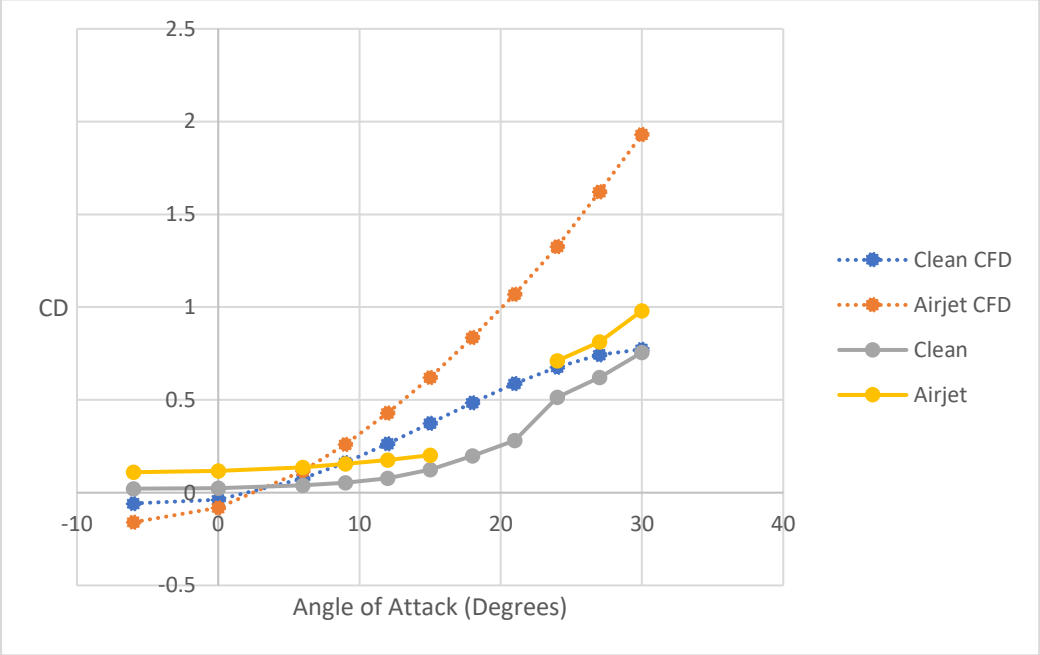


**Figure 10:** Comparison of Coefficient of Drag of CFD and experimental data.

Although the results exhibit moderately similar trendlines and proportionality to the AoA, their magnitudes differed significantly. In the drag figure, values are nearly 40-100% larger for the CFD results. As for the lift graph the CFD results tend to be underestimated but to a lesser extent. This level of discrepancy isn't unusual as we are simulating a 3D wing in 2D, the turbulence regime and solver include simplifications and most important is the use of a steady state solver when flow separation is inherently unstable and transient. The velocity of the airjet is Mach 0.60 which is encroaching compressibility effects which the solver doesn't cater for in this CFD either.



Liam Huckle mn19lth@leeds.ac.uk 201355349

## 5.3 CFD Results

**Figure 11:** Comparison of clean aerofoil with the active flow aerofoil at various Angles of Attack

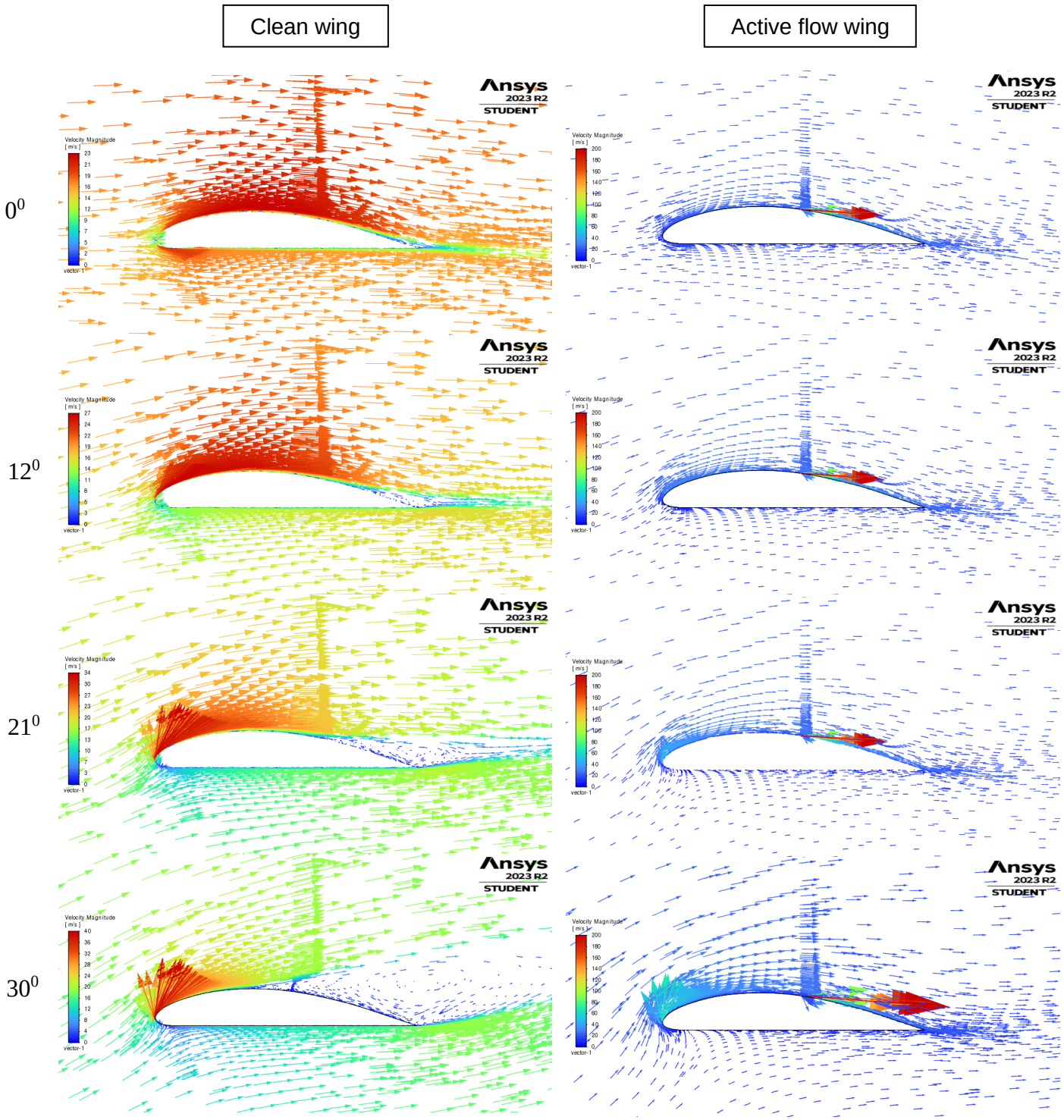




Liam Huckle mn19lth@leeds.ac.uk 201355349

**Figure 12:** Clean aerofoil X-velocity at various Angles of Attack (showing values between -5 m/s and 0 m/s)

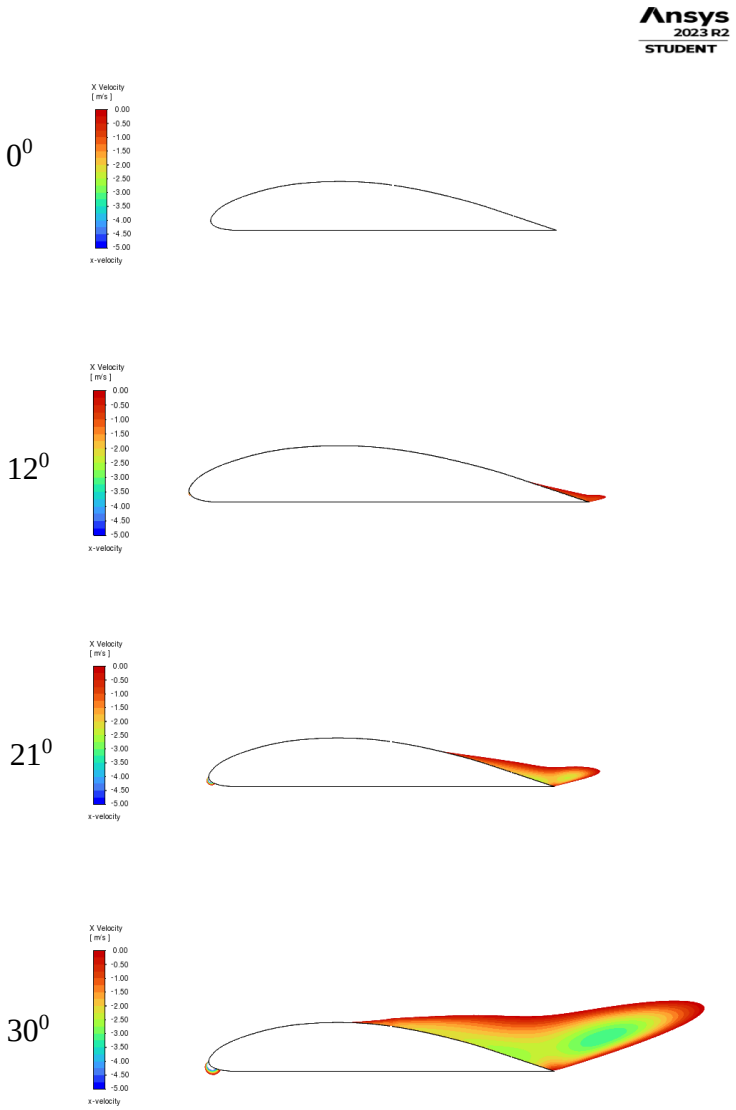


The active aerofoil wing is effective as there has been no flow separation at any of the AoAs simulated. It would appear that the critical AoA at which the wing will stall for the active wing is above 30 degrees.

The clean wing exhibits a more expected result of a growing reversed flow region behind the detachment point and increases with AoA as can be seen in figure 10. In table 3, the locations relative to the chord length were tabulated.

**Table 3:** Location of flow separation for clean configuration (Quantitative analysis)

| AoA (Degrees) | Location of flow separation (% Chord) |
|---|---|
| 0 | No flow separation |
| 12 | 94 |
| 21 | 80 |
| 30 | 56 |



Liam Huckle mn19lth@leeds.ac.uk 201355349

### 5.4 Summary of Observed Flow Features

1. Boundary layers forming on all walls.
2. Stagnation point on the leading edge (0 AoA)
3. Flow separation/detachment on top surface near trailing edge
4. Flow attachment after jet
5. Recirculation after flow separation near trailing edge at high AoA

## 6. CONTROL OF ERRORS AND UNCERTAINTY

### 6.1.1 Errors

Round off errors were minimised by setting Ansys Fluent to Double precision so 16 significant figures are used instead of 8 in single precision.

Convergence error was minimised by using plot graphs of the values of interest (lift and drag) and ensuring that these values had plateaued/converged before saving the results. This was also done by monitoring the residuals until they had levelled off, but this does not always correlate to convergence and using solution variable monitoring is more reliable.

**Figure 13:** Example of residuals when calculating the active flow wing at various angles of attack.

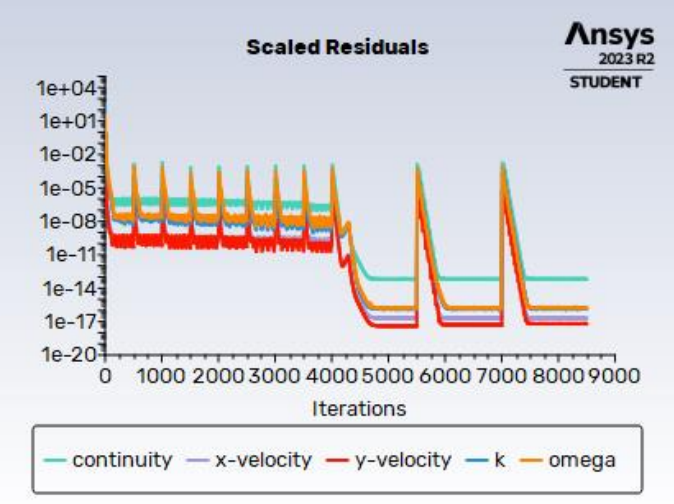


Discretisation error was evaluated using the Grid Convergence Index (GCI). The first step in minimising these errors was by ensuring the mesh was as fine as possible within the confines of computing power available. Additionally, a large safety factor of 3 was used in the GCI to account for the level of uncertainty in the CFD solutions.

The various meshes were checked for solution variable convergence and found that the difference in output was minor for the more fine meshes indicating that they were in the asymptotic range of convergence. The coarsest mesh, however, was not in this range.

The meshes were also below a max skewness of 0.51, thus further reducing solution errors as a result of poor cell geometry.

**Figure 14:** Mesh metric of skewness for fine mesh

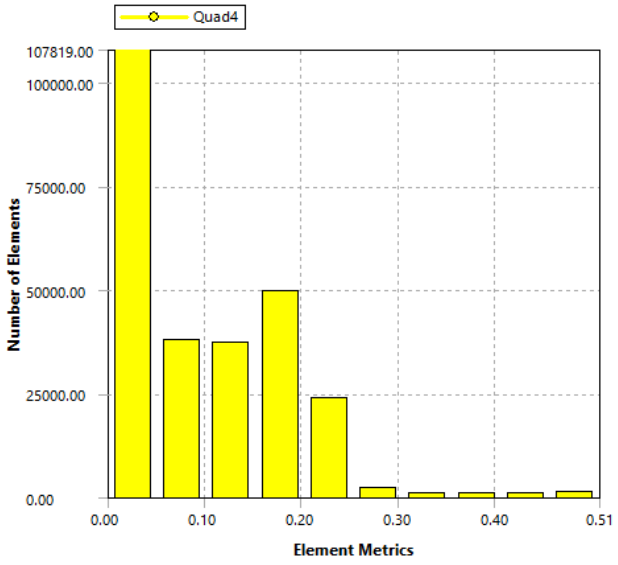


### 6.2.1 Uncertainty

Many assumptions were made about the fluid domain.

1. The flow is incompressible.
2. There is no energy or heat in the system.
3. Gravity was neglected.
4. Flow was assumed to be steady state and not transient.
5. Turbulence intensity for the inlet jet was assumed to be the same as the general inlet.
6. The fluid domain is limited to 2D.



Liam Huckle mn19lth@leeds.ac.uk 201355349

Other notable points that could lead to errors and discrepancy is the altercation of the aerofoil trailing edge to aid in grid alignment. This altered the length of the chord and the chord pitch angle. For many of the calculations the original chord length was still employed and refenced in the CFD boundary conditions. This was done for the sake of consistency and reducing the number of variables changed.

## 7. REFERENCES

1. *Cadence | Compute Grid Spacing for a Given Y+* | (2023). Available at:https://www.cadence.com/en_US/home/tools/system-analysis/computational-fluid-dynamics/y-plus.html